THE SEA: THE CURRENT AND FUTURE OCEAN
Journal of Marine Research, 77, Supplement, 247–258, 2019

Estimating particle export flux from satellite observations: Challenges associated with spatial and temporal decoupling of production and export

by Dennis J. McGillicuddy, Jr.,[1,2] Laure Resplandy,[3] and Marina Lévy[4]

ABSTRACT

Recent studies have suggested that accurate predictions of particle export flux can be derived from satellite-based estimates of phytoplankton biomass and net primary production (NPP), combined with models of the food web. We evaluate the performance of this approach using the output of a high-resolution, basin-scale coupled physical-biogeochemical model. There is tight correlation between the annual mean export flux simulated by the biogeochemical model and that predicted by the satellite-based algorithm driven by NPP from the model. Although the satellite-based approach performs well on the annual average, there are significant departures during the course of the year, particularly in spring. NPP and export flux can also become decoupled at the mesoscale, when the dynamics of fronts and eddies cause export to be displaced in space and/or time from the productivity event generating the particulate material. These findings have significant implications for the design of field studies aimed at reducing uncertainties in estimates of export flux.

Keywords: Export flux, primary production, models, remote sensing

1. Introduction

Improvements in remote sensing technology have led to increasingly sophisticated retrievals of surface ocean bio-optical properties, including not only chlorophyll absorption but also particulate backscatter and net primary production (NPP; Behrenfeld et al. 2005). These capabilities have facilitated novel approaches to estimating biogeochemical fluxes from satellite observations. In one such application, Siegel et al. (2014) combine satellite-based estimates of phytoplankton biomass and NPP with a food web model to predict the gravitational export flux of particles, hereafter referred to as simply "export flux" (Fig. 1a). Initial results of this approach are encouraging, insofar as the model predicts large-scale

1. Department of Applied Ocean Physics and Engineering, Woods Hole Oceanographic Institution, Woods Hole, MA 02543; orcid: 0000-0002-1437-2425
2. Corresponding author: ***e-mail: dmcgillicuddy@whoi.edu***
3. Geosciences Department, Princeton Environmental Institute, Princeton University, Princeton, NJ 08544; orcid: 0000-0002-1212-3943
4. Sorbonne Université, CNRS, IRD, MNHN, LOCEAN-IPSL, Paris, France; orcid: 0000-0003-2961-608X

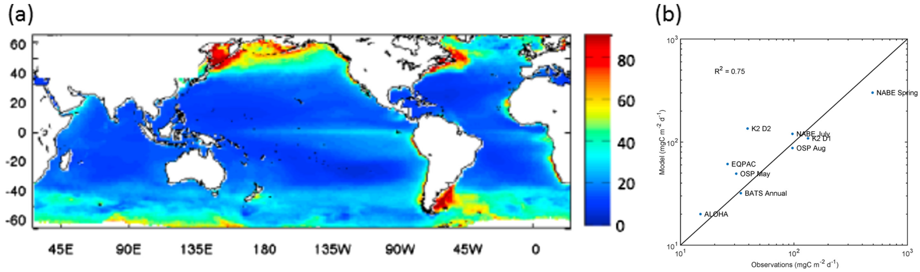

Figure 1. Results of the Siegel et al. (2014) export model. (a) Global distribution of annual mean export at 100 m (mg C m^{-2} d^{-1}). (b) Comparison of predicted and observed export at various sites. Figures 5(c) and 6(b) from Siegel et al. (2014); reproduced with permission. NABE: North Atlantic Bloom Experiment; OSP: Ocean Station Papa; EQPAC: Equatorial Pacific; ALOHA: A Long-term Oligotrophic Habitat Assessment; BATS: Bermuda Atlantic Time-series Study

trends in export flux among the relatively few places in the world ocean where particle flux data are sufficient to constrain the model (Fig. 1b).

Model-based frameworks offer a useful complement to evaluating such algorithms, insofar as they provide an internally consistent set of four-dimensional (space-time) fields that can be sampled without error at arbitrary resolution as fine as the native grid. This provides the opportunity to extract inputs to a satellite-based algorithm from a coupled physical-biogeochemical model solution, predict export using the satellite-based algorithm, and then compare with the actual export predicted by the biogeochemical model. Of course, the efficacy of this approach depends on the degree to which the biogeochemical model is an accurate representation of the real ocean. Herein we use a high-resolution biogeochemical model configured in an idealized geometry of the North Atlantic Ocean (Lévy et al. 2010). Despite its idealized geometry, the model is able to capture key aspects of observations of export flux (Resplandy et al. 2012). Although it is clearly not a perfect model, it offers a framework within which to investigate the spatial and temporal scales in which NPP and export are coupled and decoupled.

2. Methods

The model configuration features a seasonally varying, semirealistic Northwest Atlantic with a baroclinically unstable jet (the model's Gulf Stream) separating a warm, oligotrophic subtropical gyre south of the jet from a colder and more productive subpolar gyre north of it (Fig. 2). See Lévy et al. (2010, 2012) for full details on the model. The model domain is a rectangle of dimensions 2,000 km × 3,000 km, of 4 km depth, rotated by 45° on the beta-plane, with closed boundaries. The primitive equation ocean circulation model NEMO (Nucleus for European Modeling of the Ocean; Madec 2008) is used. The physical model is forced at the surface with seasonal buoyancy fluxes, solar radiation, and wind. These fluxes drive the circulation at the scale of the two gyres, generate a strong jet that runs diagonally across the domain and separates the two gyres, and also drive deep convection in the north

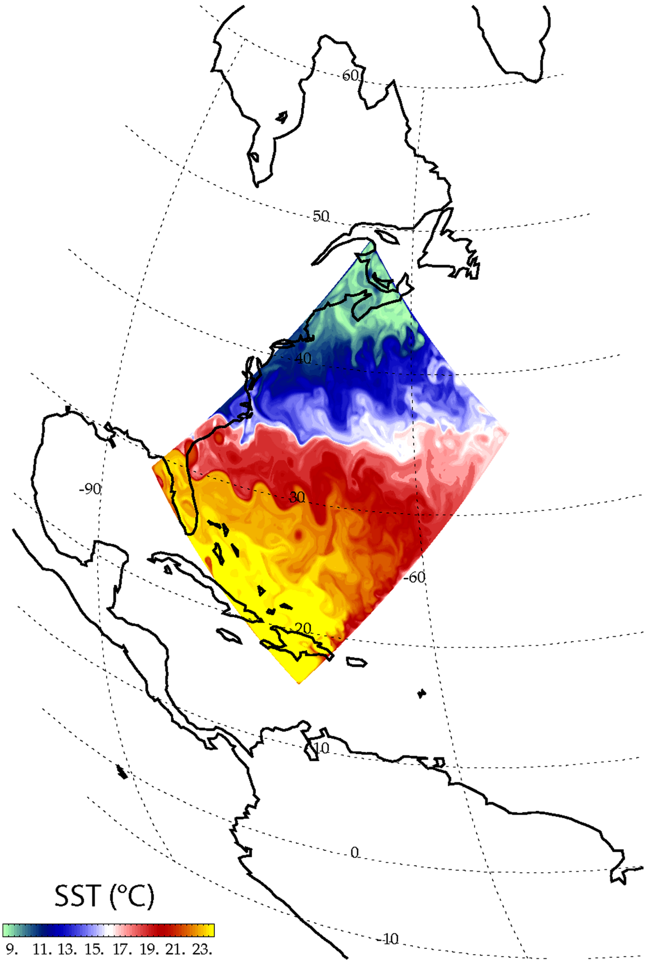

Figure 2. A snapshot of sea surface temperature (SST) in the idealized model domain representative of the western sector of the North Atlantic. Figure from Lévy and Martin (2013); reproduced with permission.

and a seasonally varying surface mixed layer. The horizontal grid resolution of the physical model is 1/54°, which permits description of the mesoscale and submesoscale features of the flow. There are 30 vertical levels. Instability processes lead to mesoscale turbulence characterized by a large number of interacting mesoscale eddies and submesoscale fronts, particularly in the band around the jet.

Coupled to this physical model is an ecosystem/biogeochemistry model, "LOBSTER." The biogeochemical model is run offline at 1/9° resolution with archived fields coarsened from the 1/54° physical model; 1/9° corresponds to the effective resolution of the physical model (Lévy et al. 2012), which means that scales finer than 1/9° are not well resolved in the physical model at 1/54°. Therefore, off-line tracer fields computed at 1/54° are very similar to those coarsened to 1/9° (Lévy et al. 2012). LOBSTER is based on a phytoplankton-zooplankton-detritus-ammonium-nitrate-labile dissolved organic nitrogen model with modules for CO_2 air-sea fluxes and ^{234}Th scavenging and export (Resplandy et al. 2009, 2012; Karleskind, Lévy, and Mémery 2011; Lévy et al. 2012).

Our satellite-based approach follows Siegel et al. (2014), in which the total export from the euphotic zone (TotEZ) is the sum of algal (AlgEZ) and zooplankton (FecEZ) contributions. AlgEZ is a constant fraction of NPP by large phytoplankton (AlgEZ = $f_{\mathrm{Alg}} \times \mathrm{NPP}_M$), whereas FecEZ is predicted by a food web model that includes small and large phytoplankton, as well as microzooplankton and mesozooplankton. Siegel et al. (2014) found that grazing rates were tightly coupled to NPP (their fig. 4), suggesting that FecEZ is tightly correlated with AlgEZ. This supports the notion of a simpler model in which TotEZ is expressed as a fraction of AlgEZ only, albeit with a larger export ratio to compensate for the lack of the FecEZ component. This is precisely the approach taken here to approximate the Siegel et al. (2014) method using the variables available in the LOBSTER biogeochemical model.

The LOBSTER model distinguishes between new production (NP) based on nitrate and regenerated production (RP) based on ammonium. It includes only one phytoplankton component and one zooplankton component, but it does explicitly resolve two size classes of sinking detrital particles: small (SD) and large (LD), which are subject to aggregation and disaggregation processes (Resplandy et al. 2012). We approximate the Siegel et al. (2014) model as follows:

$$\mathrm{NPP}_{\mathrm{LOBSTER}} = \mathrm{NP} + \mathrm{RP}, \tag{1}$$

$$\mathrm{TotEZ}_{\mathrm{LOBSTER}} = f_{\mathrm{LOBSTER}} \times \mathrm{NPP}_{\mathrm{LOBSTER}}, \tag{2}$$

where f_{LOBSTER} is the proportion of $\mathrm{NPP}_{\mathrm{LOBSTER}}$ that is exported through gravitational sinking of particles, roughly analogous to f_{Alg} in the Siegel et al. (2014) model. The prediction of $\mathrm{TotEZ}_{\mathrm{LOBSTER}}$ can be tested with the explicitly simulated export flux:

$$\mathrm{Export}_{\mathrm{LOBSTER}} = w_{\mathrm{SD}}\mathrm{SD} + w_{\mathrm{LD}}\mathrm{LD}, \tag{3}$$

where w_{SD} and w_{LD} are the sinking speeds of small (4 m d^{-1}) and large (50–200 m d^{-1}) detritus, respectively (Resplandy et al. 2012) The fractional error of the diagnostic prediction of export ($\mathrm{TotEZ}_{\mathrm{LOBSTER}}$) can thus be computed as follows:

$$\varepsilon = \frac{\mathrm{TotEZ}_{\mathrm{LOBSTER}} - \mathrm{Export}_{\mathrm{LOBSTER}}}{\mathrm{Export}_{\mathrm{LOBSTER}}}. \tag{4}$$

Both $\mathrm{TotEZ}_{\mathrm{LOBSTER}}$ and $\mathrm{Export}_{\mathrm{LOBSTER}}$ are computed using a depth horizon of 135 m. This depth was chosen to encompass the full euphotic zone even in the most oligotrophic regions of the North Atlantic.

Because of the differences in the underlying biological formulations of the satellite-based algorithm and biogeochemical model, this does not constitute an explicit test of the Siegel et al. (2014) algorithm. Rather, these model-based comparisons provide a means to evaluate the approach of estimating export fluxes from surface properties (namely, NPP) in a framework in which the inputs and outputs are known with certainty. As such, this analysis is intended to provide insight into the processes by which export can be coupled and/or decoupled with surface NPP, as well as the spatial and temporal scales over which the satellite-based approach applies.

3. Annual mean fluxes and seasonal variation

Annual mean NPP and export simulated by the LOBSTER model reflect expected large-scale patterns, with higher values in the subpolar gyre and lower values in the subtropics (Fig. 3, top row). There is a tight correlation between the annual mean export flux in the model and that estimated with the satellite-based approach (Fig. 4a). These results constrain the parameter f_{LOBSTER} in equation (2), facilitating explicit prediction of $\mathrm{TotEZ}_{\mathrm{LOBSTER}}$ from $\mathrm{NPP}_{\mathrm{LOBSTER}}$. Note that the magnitude of the annual mean export ratio f_{LOBSTER} is relatively high in this model, with a mean value of 0.52.

Comparisons between daily averages of export and NPP reveal considerably more scatter than the annual mean values (Fig. 4b). Much of this scatter is associated with the spring bloom (Fig. 4c), as the correlation is much tighter in the late summer (Fig. 4d). Statistics of the relationship between $\mathrm{TotEZ}_{\mathrm{LOBSTER}}$ and $\mathrm{Export}_{\mathrm{LOBSTER}}$ reveal correlations ranging from 0.77 to 0.99 (Table 1). Despite this high correlation, the fractional error characteristics at any one point can be quite severe, ranging from overpredictions by a factor of 100 to underpredictions by a factor of more than 4,000. The latter are associated with cases of very low export, such that the denominator of equation (4) is close to zero.

4. Mesoscale variation

Springtime snapshots of NPP and export reveal rich mesoscale variability (Fig. 3, middle and lower columns). In fact, many of the outliers in the NPP versus export relationship are associated with fronts and eddies. To get a sense of how mesoscale dynamics can decouple NPP and export, we examine a zoomed-in view of a particular event (Figs. 5 and 6).

On 7 April, an anticyclonic eddy at approximately 33° N, 76° W with an anomalously deep mixed layer has recently spawned from the front to the north. The tendency for anticyclones to contain deep mixed layers has been observed in a number of locations (Dufois et al. 2016; Hausmann, McGillicuddy, and Marshall 2017; Gaube, McGillicuddy, and Moulin 2019). In the inner core of the simulated eddy, the mixed layer depth exceeds 200m, which is sufficiently deep to entrain high-nitrate water from the nutricline, stimulate primary production, and elevate export, even in the early stages of this eddy-induced bloom. By 27 April, the mixed layer has shoaled to above 200 m where it is no longer in contact with the nutricline. Although this ends the phase of new production in this eddy-induced bloom,

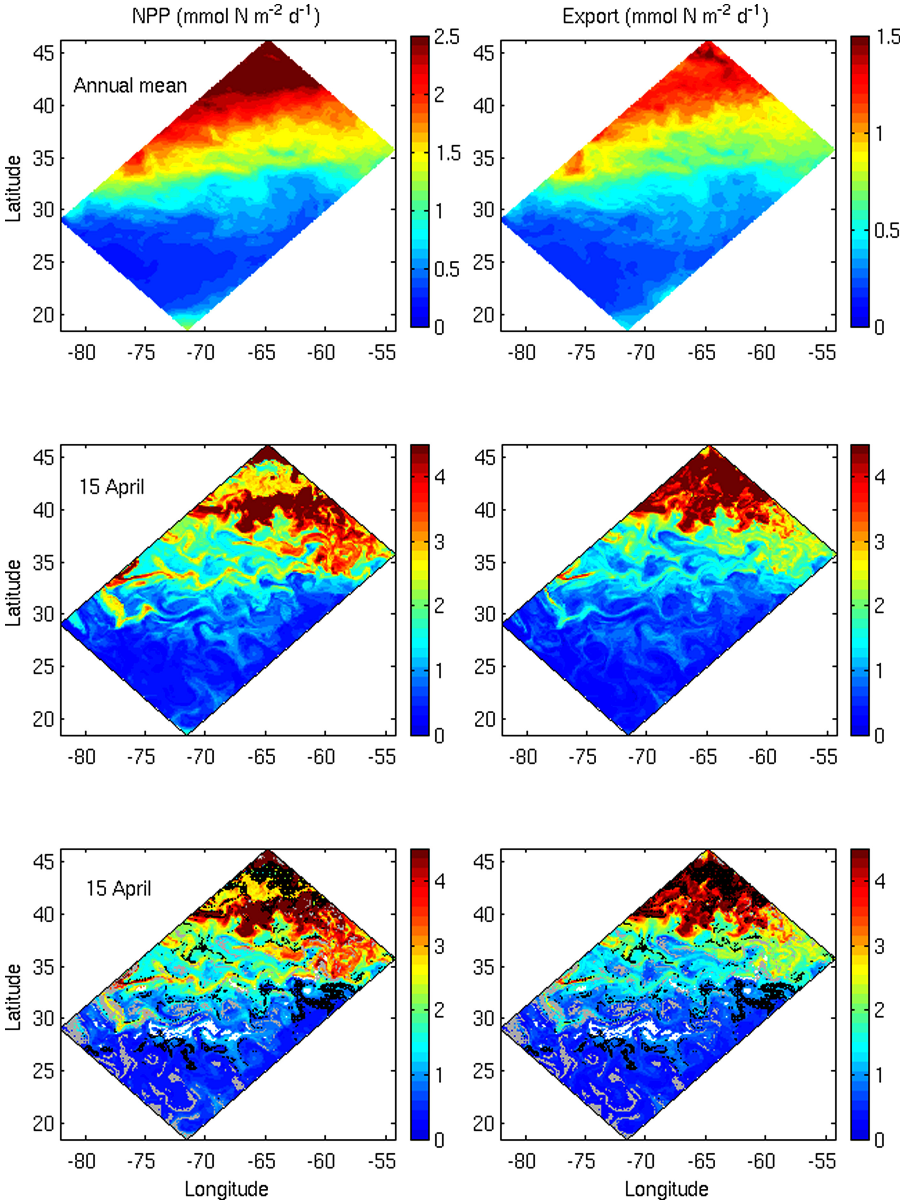

Figure 3. Net primary production (NPP) integrated over the euphotic zone (135 m) (left column) and export (right column). Top row: annual means. Middle row: a snapshot on April 15. Bottom row: same as the middle row, with the extrema in the export versus NPP relationship (binned at increments of 0.5 mmol N m^{-2} d^{-1}) shown in black (highest 10%) and gray (lowest 10%). Areas where the mixed layer depth exceeds the euphotic zone depth (135 m) are indicated in white. Note that a strip of 20 points has been removed along the lateral boundaries, so the area shown here is slightly smaller than the full domain.

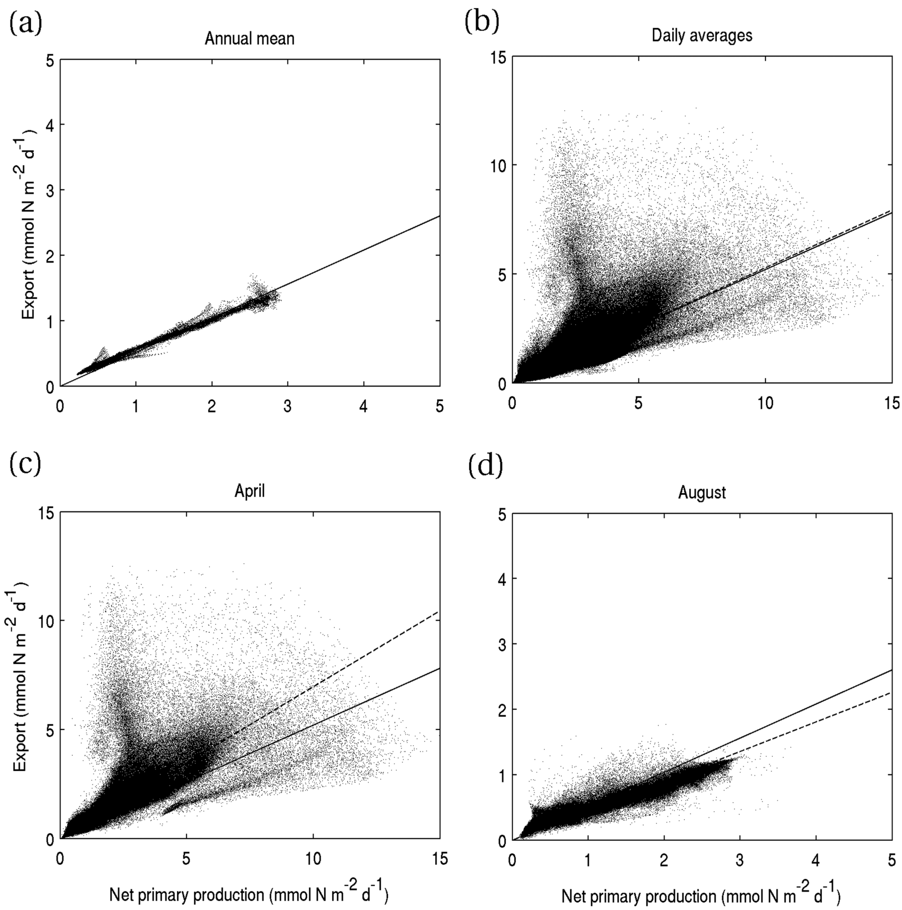

Figure 4. Scatter plots of $Export_{LOBSTER}$ (equation 3) versus the $NPP_{LOBSTER}$ (equation 1): annual mean (a) and daily averages for the entire year (b), April (c), and August (d). The solid line in the annual mean case (panel a) is replotted in panels (b)–(d) for comparison with the linear fit to the other cases (dashed lines). The slope of these linear fits is reported in Table 1 as $f_{LOBSTER}$. NPP, net primary production.

regenerated production and export continue to be enhanced. By 7 May, the mixed layer has shoaled to ∼45 m at the eddy center, reducing the amplitude of the mesoscale variation in mixed layer depth to ∼15 m. Both NPP and export decline relative to their values on 27 April, but the decline in NPP is more precipitous. As such, the enhanced export in the core of the eddy is identified as an outlier in the NPP versus export relationship (black hatching in Fig. 5). This is a direct result of the temporal decoupling in production and export associated with the eddy-induced bloom. It is interesting to note that there is spatial

Table 1. Statistics of the satellite-based algorithm applied to the biogeochemical model. The first two columns report the correlation between $TotEZ_{LOBSTER}$ (equation 2) and $Export_{LOBSTER}$ (equation 3) along with the slope of the best-fit line in each case. The fractional error computations (equation 4) utilize the annual mean $f_{LOBSTER}$. The top two rows and April and August cases correspond directly to Figure 4(a)–(d), respectively. As in Figure 4(c) and (d), all of the monthly cases reported here are daily average values. TotEZ, total export from the euphotic zone.

			Fractional error characteristics		
	$f_{LOBSTER}$	r^2	Minimum	Maximum	Standard deviation
Annual mean	0.52	0.99	−0.30	0.98	0.18
Daily averages	0.53	0.86	−4,322.4	106.5	2.38
January	0.47	0.97	−4,322.4	9.23	8.12
February	0.47	0.96	−397.3	106.5	0.74
March	0.51	0.92	−8.4	32.9	0.38
April	0.70	0.79	−0.7	21.0	0.68
May	0.57	0.77	−2.0	21.1	0.57
June	0.45	0.96	−0.8	2.8	0.35
July	0.44	0.98	−0.7	3.5	0.31
August	0.45	0.97	−0.9	7.3	0.30
September	0.47	0.97	−0.7	8.3	0.31
October	0.50	0.95	−0.7	7.1	0.29
November	0.50	0.94	−0.8	5.2	0.28
December	0.45	0.93	−12.2	6.8	0.30

decoupling as well. From a Lagrangian perspective, the eastward propagation of the eddy feature results in export of material more than 200 km from the point of origin of the eddy.

5. Conclusions

Prediction of export flux from satellite observations is appealing for a number of reasons, not the least of which is the spatial and temporal coverage of the surface ocean properties provided by remote sensing (Siegel et al. 2014). Testing of such models presents a formidable challenge, insofar as the spatial and temporal scales accessible with in situ observations is much more limited. Ongoing efforts such as the Export Processes in the Ocean from Remote Sensing (EXPORTS) program (Siegel et al. 2016) seek to expand the observational basis for such approaches.

Herein we offer a model-based framework to assess the degree of coupling between NPP (observable by satellite) and export. On an annual mean basis, export is well correlated with NPP, and robust predictions can be made on a point-by-point basis. However, strong seasonality of the temperate ocean creates temporal decoupling between production and export on seasonal timescales, and the quality of monthly predictions is substantially degraded over large regions of the ocean during the spring bloom. Mesoscale flows also introduce perturbations to the system, creating hot spots in productivity for which the subsequent

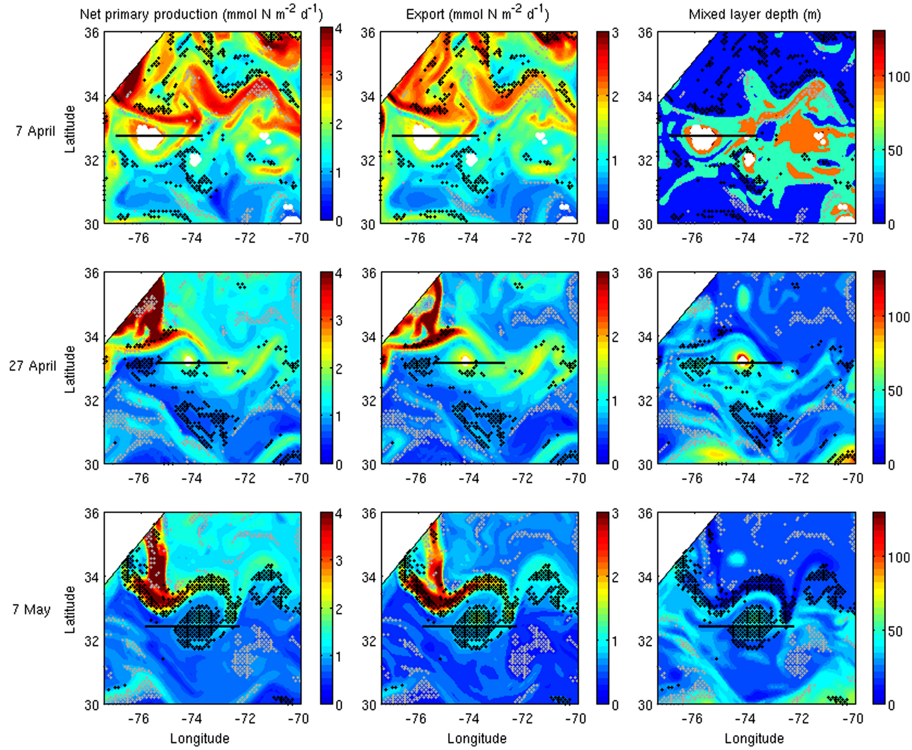

Figure 5. Zoomed-in view of a mesoscale export event. Net primary production (NPP; left column), export (middle column), and mixed layer depth (right column) on 7 April (top row), 27 April (middle row), and 7 May (bottom row). Extrema in the export versus NPP relationship (binned at increments of 0.5 mmol N m^{-2} d^{-1}) are shown in black (highest 10%) and gray (lowest 10%). Areas where the mixed layer depth exceeds the euphotic zone depth (135 m) are indicated in white. Solid black lines indicate the locations of the cross sections shown in Figure 6.

export is spatially and temporally displaced from the point of origin. Despite the relatively fine resolution of the present model, we expect even finer-scale fluctuations in export flux associated with the submesoscale (Estapa et al. 2015; Omand et al. 2015; Stukel et al. 2017; Erickson and Thompson 2018). Moreover, treatment of subduction of both particulate and dissolved materials will be required for more complete models of total export flux (Boyd et al. 2019; Resplandy, Lévy, and McGillicuddy 2019). Of course, top-down control by the community of grazers provides yet another means for decoupling primary production and export (Banse 1992). In any case, the present results highlight the wide range of spatial and temporal scales that must be resolved in order to evaluate satellite-based predictions of export flux.

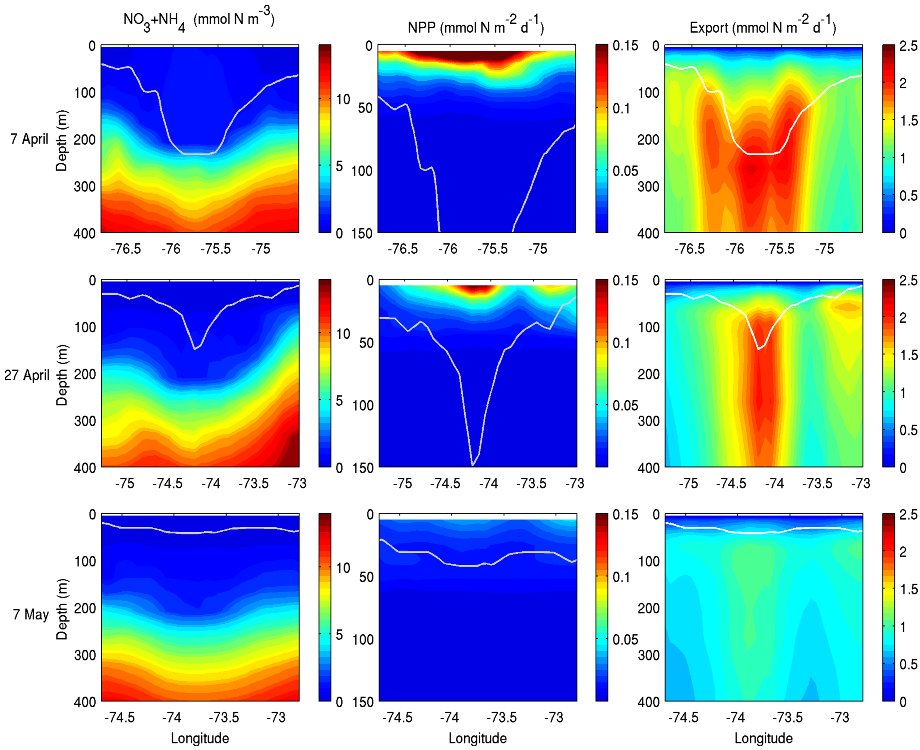

Figure 6. Cross sections of nitrate plus ammonium (left column), net primary production (NPP; middle column), and export (right column) on 7 April (top row), 27 April (middle row), and 7 May (bottom row). The thin white line in each panel indicates the depth of the mixed layer. Locations of the cross sections for each date are shown as solid black lines in Figure 5. Note the shallower vertical scale of the right column.

Acknowledgments. DJM gratefully acknowledges National Aeronautics and Space Administration (NASA) grant NNX16AR50G and support from the National Science Foundation. LR is funded by NASA EXPORTS awards 80NSSC17K0555 and NNX16AR50G. ML is supported by Centre National d'Etudes Spatiales (CNES) and by the French Agence Nationale de la Recherche award SOBUMS award ANR-16-CE01-0014. We thank Valery Kosnyrev for his excellent analysis and visualization of the results presented herein. It is with deepest gratitude that DJM offers this work in tribute to his graduate adviser Professor James J. McCarthy. McCarthy's intellectual guidance played a foundational role in shaping the interdisciplinary basis for DJM's career, and his mentorship provided ongoing inspiration for a lifelong quest to understand physical-biological interactions in the ocean.

REFERENCES

Banse, K. 1992. Grazing, temporal changes of phytoplankton concentrations, and the microbial loop in the open sea, *in* Primary Productivity and Biogeochemical Cycles in the Sea, P. G. Falkowski, A. D. Woodhead, and K. Vivirito, eds. Boston, MA: Springer, 409–440.

Behrenfeld, M. J., E. Boss, D. A. Siegel, and D. M. Shea. 2005. Carbon-based ocean productivity and phytoplankton physiology from space. Global Biogeochem. Cycles, *19*, GB1006. doi: 10.1029/2004GB002299

Boyd, P. W., H. Claustre, M. Lévy, D. A. Siegel, and T. Weber. 2019. Multi-faceted particle pumps drive carbon sequestration in the ocean. Nature, *568*, 327–335. doi: 10.1038/s41586-019-1098-2

Dufois, F., N. J. Hardman-Mountford, J. Greenwood, A. J. Richardson, M. Feng, and R. J. Matear. 2016. Anticyclonic eddies are more productive than cyclonic eddies in subtropical gyres because of winter mixing. Sci. Adv., *2*, e1600282. doi: 10.1126/sciadv.1600282

Erickson, Z. K., and A. F. Thompson. 2018. The seasonality of physically driven export at submesoscales in the northeast Atlantic Ocean. Global Biogeochem. Cycles, *32*, 1144–1162. doi: 10.1029/2018GB005927

Estapa, M. L., D. A. Siegel, K. O. Buesseler, R. H. R. Stanley, M. W. Lomas, and N. B. Nelson. 2015. Decoupling of net community and export production on submesoscales in the Sargasso Sea. Globa; Biogeochem. Cycles, *29*, 1266–1282. doi: 10.1002/2014GB004913

Gaube, P., D. J. McGillicuddy, and A. J. Moulin. 2019. Mesoscale eddies modulate mixed layer depth globally. Geophys. Res. Lett., *46*, 1505–1512. doi: 10.1029/2018GL080006

Hausmann, U., D. J. McGillicuddy, and J. Marshall. 2017. Observed mesoscale eddy signatures in Southern Ocean surface mixed-layer depth. J. Geophys. Res.: Oceans, *122*, 617–635. doi: 10.1002.2016JC012225

Karleskind, P., M. Lévy, and L. Mémery. 2011. Subduction of carbon, nitrogen, and oxygen in the northeast Atlantic. J. Geophys. Res.: Oceans, *116*, C02025. doi: 10.1029/2010JC006446

Lévy, M., D. Iovino, L. Resplandy, P. Klein, G. Madec, A. M. Tréguier, S. Masson, and K. Takahashi. 2012. Large-scale impacts of submesoscale dynamics on phytoplankton: Local and remote effects. Ocean Modell., *43–44*, 77–93. doi: 10.1016/j.ocemod.2011.12.003

Lévy, M., P. Klein, A. M. Tréguier, D. Iovino, G. Madec, S. Masson, and K. Takahashi. 2010. Modifications of gyre circulation by sub-mesoscale physics. Ocean Modell., *34*, 1–15. doi: 10.1016/j.ocemod.2010.04.001

Lévy, M., and A. P Martin. 2013. The influence of mesoscale and submesoscale heterogeneity on ocean biogeochemical reactions. Global Biogeochem. Cycles, *27*, 1139–1150. doi: 10.1002/2012GB004518

Madec, G. 2008. Nemo Ocean Engine. Note du Pole de modelisation 27. Paris: Institut Pierre-Simon Laplace.

Omand, M. M., E. A. D'Asaro, C. M. Lee, M. J. Perry, N. Briggs, I. Cetiniæ, and A. Mahadevan. 2015. Eddy-driven subduction exports particulate organic carbon from the spring bloom. Science, *348*, 222–225. doi: 10.1126/science.1260062

Resplandy, L., M. Lévy, F. d'Ovidio, and L. Merlivat. 2009. Impact of submesoscale variability in estimating the air-sea CO_2 exchange: Results from a model study of the POMME experiment. Global Biogeochem. Cycles, *23*, GB1017. doi: 10.1029/2008GB003239.

Resplandy, L., M. Lévy, and D. J. McGillicuddy, Jr. 2019. Effects of eddy-driven subduction on ocean biological carbon pump. Global Biogeochem. Cycles, *33*, 1071–1084. doi: 10.1029/2018GB006125

Resplandy, L., A. P. Martin, F. Le Moigne, P. Martin, A. Aquilina, L. Mémery, M. Lévy, and R. Sanders. 2012. How does dynamical spatial variability impact 234Th-derived estimates of organic export? Deep-Sea Res., Part I, *68*, 24–45. doi: 10.1016/j.dsr.2012.05.015

Siegel, D. A., K. O. Buesseler, M. J. Behrenfeld, C. R. Benitez-Nelson, E. Boss, M. A. Brzezinski, A. Burd, et al. 2016. Prediction of the export and fate of global ocean net primary production: The EXPORTS science plan. Front. Mar. Sci., *3*, 22. doi: 10.3389/fmars.2016.00022

Siegel, D. A., K. O. Buesseler, S. C. Doney, S. F. Sailley, M. J. Behrenfeld, and P. W. Boyd. 2014. Global assessment of ocean carbon export by combining satellite observations and food-web models. Global Biogeochem. Cycles, *28*, 181–196. doi: 10.1002/2013gb004743

Stukel, M. R., L. I. Aluwihare, K. A. Barbeau, A. M. Chekalyuk, R. Goericke, A. J. Miller, M. D. Ohman, et al. 2017. Mesoscale ocean fronts enhance carbon export due to gravitational sinking and subduction. Proc. Natl. Acad. of Sci. U. S. A., *114*, 1252–1257. doi: 10.1073/pnas.1609435114

Received: *1 May 2019*; revised: *25 June 2019*.